Journal of the Ceramic Society of Japan 133 [9] 488-496 2025
DOI https://doi.org/10.2109/jcersj2.25038

JCS-Japan

REVIEW

Hyperordered structures in silica polymorphs

Shinji Kohara[1,†]

[1]Center for Basic Research on Materials, National Institute for Materials Science, Tsukuba, Ibaraki 305–0047, Japan

We have been exploring with the quest hyperordered structures in terms of order within disorder in silica (SiO_2) polymorphs. In this article, we review and discuss our recent findings on this topic comprehensively in comparison with those of previous studies. We chose several SiO_4 tetrahedral corner-sharing crystalline silica and siliceous zeolites of various density. Furthermore, we attempted to control the intermediate-range ordering of glass by tuning of the density of silica glass under high pressures and temperatures. We extracted the density-driven modification of the topology of tetrahedral silica polymorphs in a wide density range. Our state-of-the-art analyses revealed two descriptors for hyperordered structures in silica polymorphs. The first descriptor of hyperordered structures in silica glass can be expressed by the position and height of diffraction peaks observed in X-ray and neutron diffraction data. This descriptor is not new, but we can systematically understand the density-driven behaviour of diffraction peaks in silica glass. The second descriptor of hyperordered structures in a series of silica polymorphs can be expressed in terms of topological characteristics: ring size distribution, cavity distribution, ring shape, and tetrahedral order. We found an unusually large cavity volume in β-cristobalite which was attributable to the formation of highly symmetrical –Si–O– sixfold rings, and highly symmetrical eightfold and twelvefold rings in coesite even though most of the small rings were significantly buckled, which was due to coesite having the highest density of coesite among the series of silica polymorphs. Moreover, we found a topological similarity between glass and siliceous zeolite (MFI), in which fivefold and sevenfold rings are observed. It is concluded that both diffraction measurement and topological analysis provide us crucial information on hyperordered structures in silica polymorphs.

Key-words : Densified silica glass, Silica polymorphism, Siliceous zeolite, Topology, Diffraction

[Received March 13, 2025; Accepted April 21, 2025; Published online September 1, 2025]

1. Introduction

Silica (SiO_2) polymorphisms, which are the most important solid oxides in materials and earth sciences, have been widely studied using many experimental and simulation techniques.[1,2] In contrast to crystalline silica, the structural information of the glass and liquid is insufficient owing to the limited information that can be accessed by experimental and simulation techniques. However, the recent advent of advanced quantum beam (X-rays, electrons, and neutrons) and computer simulation techniques has made feasible to obtain dependable atomic configurations.[3–9]

Quantum beam diffraction techniques can provide us direct information on the atomistic structure of glassy and liquid materials. In particular, the combination of hard X-ray diffraction measurements at synchrotron radiation sources and neutron diffraction measurements at both reactor and spallation sources is powerful because neutrons are sensitive to oxide atoms, whereas X-rays are sensitive to heavy elements.[1,2] Silica glass exhibits a three-peak structure: the first sharp diffraction peak (FSDP, $Q_1 \sim 1.5$ Å^{-1}),[10–13] in X-ray or neutron structure factor $S(Q)$, the second principal peak (PP, $Q_2 \sim 3$ Å^{-1})[12,13] in neutron $S(Q)$, and Q_3 at $Q \sim 5$ Å^{-1} in X-ray or neutron $S(Q)$. FSDP can be understood in terms of a periodicity of 4 Å ($2\pi/Q_1$) and a coherence length of 10 Å ($2\pi/\Delta Q_1$) by the peak position and width, respectively.[14] Indeed, FSDP is a signature of periodicity arising from the succession of cage structures formed by corner-sharing SiO_4 tetrahedra.[15,16]

We have been working on the synthesis of densified silica glass via hot (up to 1500 °C at 7.7 GPa) and cold (RT/20 GPa) densifications to understand the behaviour of FSDP and PP on the basis of X-ray and neutron diffraction data. Note that the density of glass recovered at >1200 °C/7.7 GPa by hot densification was identical to that of cold-densified glass. We observed that the height of FSDP and the density of the glass densified at 1300 °C/7.7 GPa were maximum, whereas the height of FSDP of the cold-densified glass was minimum.[17,18]

We have recently applied a series of topological analysis techniques for ring size distribution, cavity distribution, ring shape, and tetrahedral order to silica polymorphs. In this work, we chose several SiO_4 tetrahedral corner-sharing crystalline silica and siliceous zeolites (MFI, SOD, and FAU) of various densities to understand the density-

† Corresponding author: S. Kohara; E-mail: KOHARA.Shinji@nims.go.jp

‡ Preface for this article: DOI https://doi.org/10.2109/jcersj2.133.P9-1

driven modification of topology in a wide density range (1.33–2.91 g cm^{-3}).[19]

In this article, we review our recent findings as mentioned above and discuss the origin of hyperordered structures in silica polymorphs, and the capability of diffraction measurements and a series of topological analysis techniques.

2. Data analysis

To understand the topology of silica polymorphs, the ring size distribution, cavity distribution (surface cavity volume was calculated using a cut off distance $r_{cut} = 2.5$ Å), and ring shape [one-dimensional persistence diagram (PD),[20,21] which shows the birth and death of rings in silica polymorphs], were calculated using the R.I.N.G.S. code,[22,23] pyMolDyn code,[24] and HomCloud package,[25] respectively.

The tetrahedral order parameter q for Si-centric tetrahedra is expressed by[26]

$$q \equiv 1 - \frac{3}{8}\sum_{i=1}^{3}\sum_{k=i+1}^{4}\left(\frac{1}{3} + \cos\theta_{ijk}\right)^2, \quad (1)$$

where θ_{ijk} is the angle between the central Si atom j and its neighbouring Si atoms i and k. This parameter was designed to be unity in a regular tetrahedron and have a mean value of zero in a perfect gas.

The details of a series of analyses are described in our previous publications.[27–29]

3. Results and discussion

3.1 Hot- and cold-densified silica glasses

Figure 1(a) shows the temperature-dependent densities of the hot-densified silica glass at 7.7 GPa (black) and the cold-densified silica glass (RT/20 GPa, cyan), and those of α-cristobalite (green), α-quartz (magenta), and coesite (grey).[17] As can be seen in the figure, the density of hot-densified silica glass does not change monotonically; the density increases rapidly up to 600 °C/7.7 GPa, but increases slowly thereafter. Figure 1(b) shows the X-ray (upper) and neutron (lower) total structure factors $S(Q)$ of densified silica glasses.[17] It is well known that X-rays are more sensitive to the silicon–silicon correlation at $Q_1 \sim 1.5$ Å^{-1}, whereas neutrons are more sensitive to the oxygen–oxygen correlation at $Q_2 \sim 3$ Å^{-1} [no PP is observed in X-ray $S(Q)$],[5,17] suggesting that we should focus on the FSDP in X-ray $S(Q)$ and the PP in neutron $S(Q)$. As can be seen in Fig. 1(b), the FSDP of X-ray $S(Q)$ shifts to the high-Q side and its height decreases at 400 °C/7.7 GPa but increases at 1200 °C/7.7 GPa. This peak height change reflects the ordering of Si–Si correlation at the FSDP position according to the MD-RMC model for hot densification.[17] We suggest that the rapid increase in density is associated with the reduction in cavity volume[17] and the slow increase in density thereafter associated with the structural ordering expressed by the height of FSDP in X-ray $S(Q)$. This ordering is largely affected by the evolution

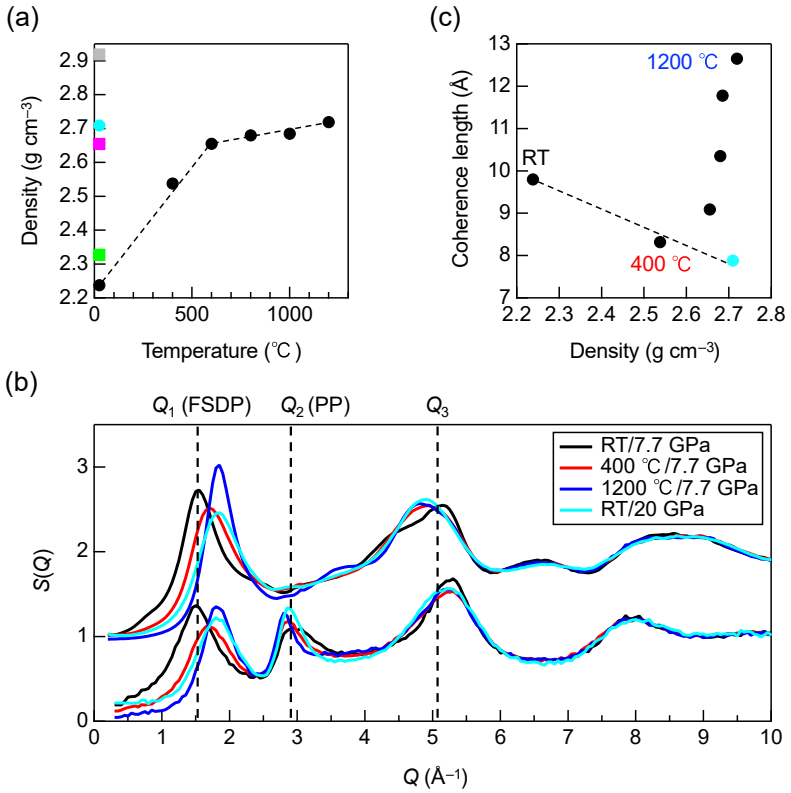

Fig. 1. (a) Temperature-dependent densities of the hot-densified silica glass at 7.7 GPa (black) and cold-densified silica glass (RT/20 GPa, cyan), and those of α-cristobalite (green), α-quartz (magenta), and coesite (grey).[17] (b) X-ray (upper) and neutron (lower) total structure factors $S(Q)$ of densified silica glasses.[17] (c) Coherence length ($2\pi/\Delta Q_1$) of the hot-densified silica glass and cold-densified glass (cyan).[17]

of the Si–Si correlation towards relaxation to the crystalline phase because no such a clear behaviour is observed in the FSDP of neutron $S(Q)$ owing to the difference in weighting factors for X-ray and neutron diffraction data. Although the diminishment of FSDP was observed in many previous studies using in situ X-ray diffraction,[30–34] in situ neutron diffraction,[35] and X-ray diffraction measurements of hot- and cold-densified glasses,[36] our finding is the first to show that the evolution of FSDP in hot-densified glass. Note that the density of hot-densified glass synthesized at 1200 °C/7.7 GPa is identical to that of cold-densified glass [cyan in Fig. 1(a)]. Nevertheless, the height of FSDP of the latter is much lower than that of the former, suggesting that we synthesized two densified silica glasses with the same density, but different structures. Figure 1(c) shows the coherence length ($2\pi/\Delta Q_1$) values of the hot (black)- and cold (cyan)-densified silica glasses,[17] demonstrating the modification of the glass structure in the intermediate-range scale by pressure and temperature. This behaviour suggests that a glass structure rejuvenates up to 400 °C/7.7 GPa and then relaxes to a coesite structure thereafter because hot-densified glass transforms into coesite when the temperature is increased. Moreover, we measured the density and X-ray diffraction data of hot- and cold-densified glasses and found that cold-densified glass is not permanently densified, which is inconsistent with previous studies.[37,38]

3.2 Amorphous silica with a zeolite like topology

Figure 2 shows the X-ray total structure factors $S(Q)$ of cold-densified silica glass[17] and cold-densified amorphous MFI obtained by cold densification of a MFI single crystal.[39,40] Note that the densities of two samples are both 2.7 g cm^{-3}. The X-ray $S(Q)$ of both samples are identical and exhibit an FSDP at $Q = 2$ Å^{-1}, although amorphous MFI has a tiny peak at around $Q \sim 0.6$ Å^{-1}, as indicated by an arrow, which corresponds to a trace of (101) and (020) reflections in crystalline MFI. **Figure 3** shows the primitive[41,42] ring size distributions (left) and atomic configurations (right) of (a) cold-densified silica glass and (b) cold-densified amorphous MFI.[40] The ring size distribution of silica glass shows a broad (threefold to tenfold) distribution, although $(Si–O)_6$ sixfold rings, which are the only rings of cristobalite,[19] are predominant. This broad distribution is topologically disordered according to Cooper.[43] Amorphous MFI also shows a broad (fourfold to tenfold) distribution, but the fraction of fivefold rings is large, which is a trace of crystalline MFI because we chose the crystal structure as an initial atomic configuration for the RMC modelling of amorphous MFI. Indeed, we could not fit the experimental diffraction data by RMC modelling when we started from a random configuration.[39] The difference in ring size distribution is found to be well reflected in the distributions in cavities; cavities of silica glass are randomly distributed, whereas those of amorphous MFI has a crystalline topology. This difference is a reason why silica glass is not permanently densified, whereas amorphous MFI formed by cold densification is stable for at least ten years[17] and has a different amorphous structure compared to cold-densified silica glass.

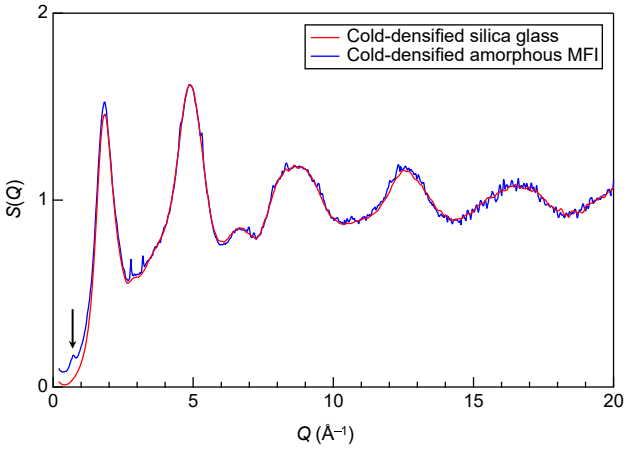

Fig. 2. X-ray total structure factors $S(Q)$ of cold-densified silica glass[17,40] and cold-densified amorphous MFI.[39,40]

3.3 Topological analyses of silica polymorphs

Figure 4 shows the crystal structures of α-cristobalite, β-cristobalite, α-quartz, coesite, FAU, SOD, and MFI together with the atomic configuration of silica glass obtained by a combination of molecular dynamics and reverse Monte Carlo[8,44] (MD–RMC) modelling.[40] Note that the density of silica glass (2.21 g cm^{-3}) is the same as that of β-cristobalite, and those of siliceous zeolites (FAU: 1.33 g cm^{-3}; SOD: 1.66 g cm^{-3}; MFI: 1.84 g cm^{-3}) are lower than that of silica glass. On the other hand, the densities of the remaining three crystalline phases (α-

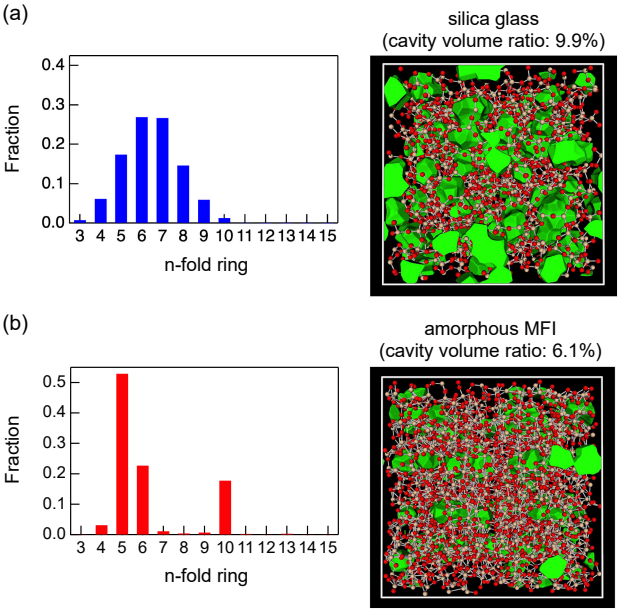

Fig. 3. Primitive ring size distributions (left) and atomic configurations (right) of (a) cold-densified silica glass and (b) cold-densified amorphous MFI.[40] Red spheres: oxygen; blue spheres: silicon. Cavities are shown in green. Note that the atomic configuration of cold-densified silica glass was obtained by MD–RMC simulation.[17]

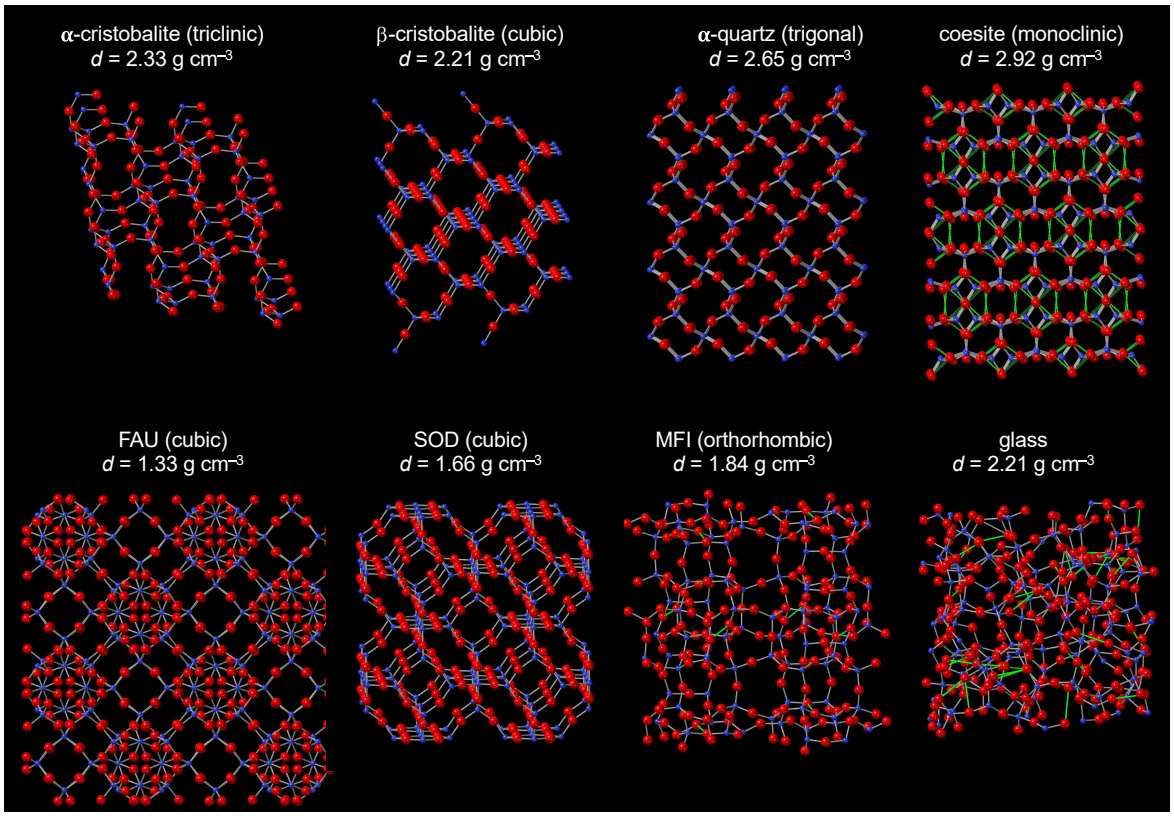

Fig. 4. Crystal structures of α-cristobalite, β-cristobalite, α-quartz, coesite, FAU, SOD, and MFI together with the atomic configuration of silica glass obtained by MD–RMC simulation.[19] Red spheres: oxygen; blue spheres: silicon. The intertetrahedral oxygen–oxygen correlations are highlighted by green sticks.

cristobalite: 2.33 g cm^{-3}; α-quartz: 2.65 g cm^{-3}; coesite: 2.92 g cm^{-3}) are higher than that of silica glass. As can be seen in Fig. 4, the intertetrahedral oxygen–oxygen correlations up to 3.2 Å, which are indicated by green sticks, are observed only in coesite, silica glass, and MFI. The behaviour of MFI might be the reason why densified amorphous MFI was permanently densified for at least 10 years by cold densification, as discussed in sect. 3.2.

A schematic of intra- and intertetrahedral oxygen–oxygen correlations in silica glass is shown in **Fig. 5**(a) as an example.[19] These correlations are observed only in coesite, silica glass, and MFI. Since coesite has the highest density among silica polymorphs, an intertetrahedral oxygen–oxygen correlation is formed at a high density. In the case of silica glass, an intertetrahedral oxygen–oxygen correlation is the result of disorder. However, it is difficult to form an intertetrahedral oxygen–oxygen correlation in MFI because density is very low compared with those of coesite and silica glass.

Here, we discuss the origins of FSDP and PP. Figure 5(b) shows the schematic illustrations of β-cristobalite with the assignment of FSDP and PP proposed by Benmore and Wilding.[45] As discussed in sect. 3.1, the periodicity estimated by the position of FSDP in silica glass is 4 Å ($2\pi/Q_1$), which corresponds to that of dFSDP in Fig. 5(b). They assigned the coherence length of 2 Å ($2\pi/Q_2$) to the distance from the base to the apex of a SiO_4 tetrahedron (dPP) as suggested by Salmon and Zeidler.[13] However, this interpretation cannot explain the reason why the PP of silica glass evolved under high pressures at room temperature,[35] where the Si–O coordination number remained to be four. We suggest that the ordering of intertetrahedral oxygen–oxygen correlation under high pressures associated with the reduction in cavity volume, as illustrated in Fig. 5(c), is the origin of the evolved PP under high pressures. This hypothesis is in line with the density increase shown in Fig. 1(a). The origin of Q_3 was discussed in Ref. 14, in which the succession of nearest neighbour correlations can reproduce Q_3.

Figure 6 shows the oxygen–oxygen total correlation functions $T_{OO}(r)$ (a) and intratetrahedral oxygen–oxygen total correlation functions $T^{intra}{}_{OO}(r)$ (b) of hot-densified silica glasses obtained by MD-RMC simulation. Note that $T^{intra}{}_{OO}(r)$ were calculated by using only the intrateraheral oxygen–oxygen correlations. A prominent correlation peak is found at 2.6 Å, and a subtle second oxygen–oxygen correlation peak is observed at ~3.5 Å, whose height increases with temperature (density), whereas $T^{intra}{}_{OO}(r)$ remains the same, suggesting that only the intertetraheral oxygen–oxygen correlation evolved by hot densification. This behaviour is in line with the behaviour of the PP shown in Fig. 1(c), in which the PP shifts to the low-Q side caused by the evolution of the height of the peak observed at 3.5 Å in $T_{OO}(r)$ by hot densification.

Figure 7 shows the cavity distributions in silica polymorphs[19] and **Table 1** summarizes the densities and cav-

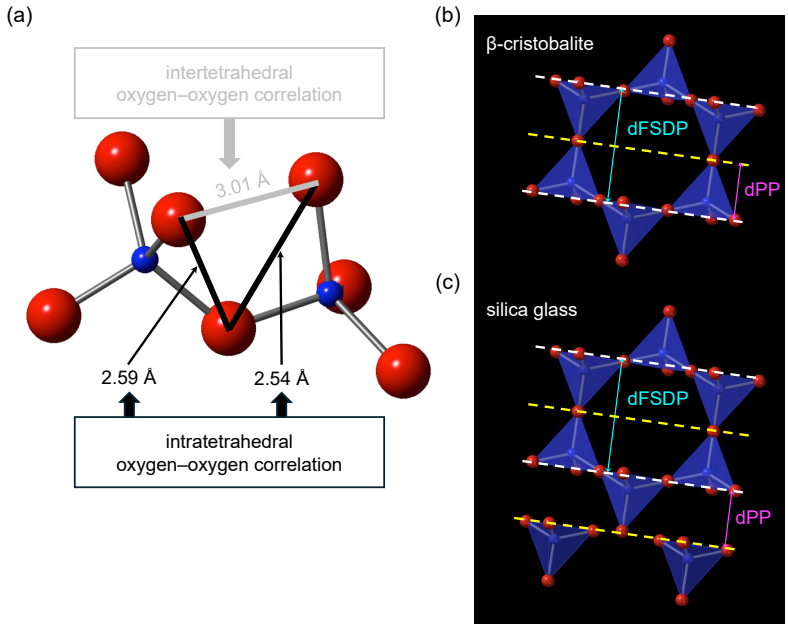

Fig. 5. (a) Schematic of intra- and intertetrahedral oxygen–oxygen correlations in silica glass.[19] Blue: Si; red: O. Schematic illustrations of β-cristobalite (b) and silica glass (c) with the coherence lengths of FSDP and PP.

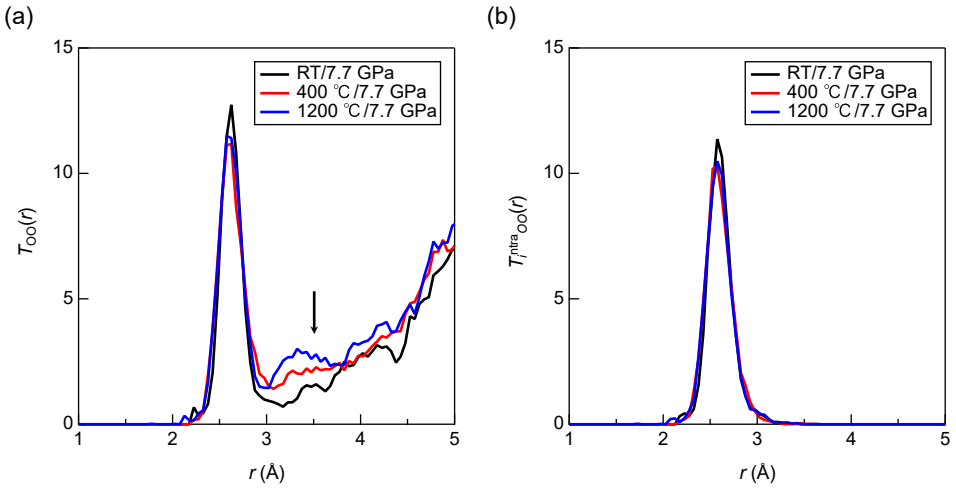

Fig. 6. Oxygen–oxygen total correlation functions $T_{OO}(r)$ (a) and intratetrahedral oxygen–oxygen total correlation functions $T^{intra}{}_{OO}(r)$ (b) of hot-densified silica glasses obtained by MD–RMC simulation.

ity volume ratios of silica polymorphs. It is found that the cavity volume ratio of β-cristobalite (54 %), whose density is identical to that of silica glass, is higher than those of silica glass (33 %) and MFI (47 %). On the other hand, we observe no cavities in α-cristobalite, α-quartz, and coesite. Moreover, FAU has the highest cavity volume ratio (69 %) because it has the lowest density among the silica polymorphs. A series of analyses suggest that the cavity volume ratio of β-cristobalite is comparable to those of siliceous zeolites, which agrees with Gaskell and Wallis's argument,[46] on the basis of which they reported the structural similarity between silica glass and β-cristobalite in terms of the peak position in diffraction data.

Figure 8 shows the O-centric PDs for α-cristobalite, β-cristobalite, α-quartz, coesite, FAU, SOD, MFI, and silica glass.[19] The O-centric PD is important in understanding the packing fraction of oxygen atoms[47] in oxide materials. All PDs exhibit prominent profiles at $b_k \sim 1.6$ Å^2. A similar behaviour between α- and β-cristobalites is found in the Si-centric PDs,[19] but no such similarity is observed in the O-centric PDs, although the O-centric PD is identical between α- and β-quartz. A long lifetime ($= d_k - b_k$)[28] profile observed at $b_k/d_k = 1.45$ Å^2/6.20 Å^2 in the O-centric PD for β-cristobalite shows that the sixfold rings are very symmetrical in β-cristobalite. It is also suggested that this long lifetime profile is the reason for the high cavity volume ratio in β-cristobalite. As can be seen in Fig. 8, the O-centric PD for SiO_2 silica glass shows a prominent vertical profile along with the d_k axis at $b_k \sim 1.7$ Å^2. For siliceous zeolites, no systematic change can be observed in the PDs; the O-centric PD for FAU has a long lifetime profile at $b_k/d_k = 1.4$ Å^2/24.5 Å^2, indicating that a large

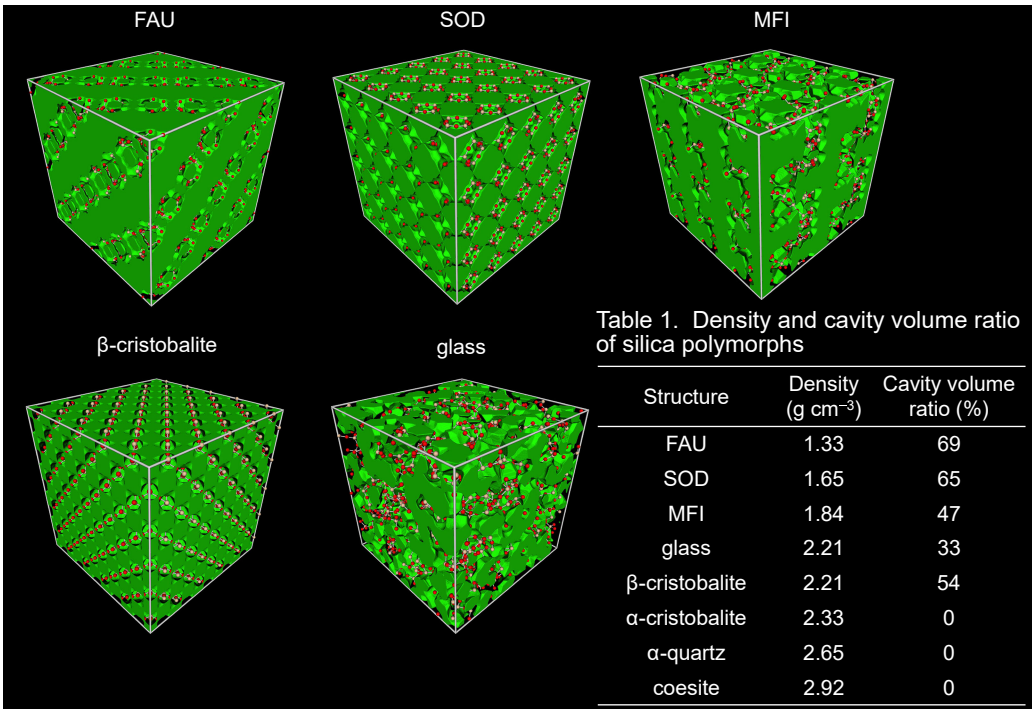

Table 1. Density and cavity volume ratio of silica polymorphs

Structure	Density (g cm^{-3})	Cavity volume ratio (%)
FAU	1.33	69
SOD	1.65	65
MFI	1.84	47
glass	2.21	33
β-cristobalite	2.21	54
α-cristobalite	2.33	0
α-quartz	2.65	0
coesite	2.92	0

Fig. 7. Cavity distribution in a series of silica polymorphs.[19] Cavities are shown in green. Red sphere: oxygen; pink sphere: silicon.

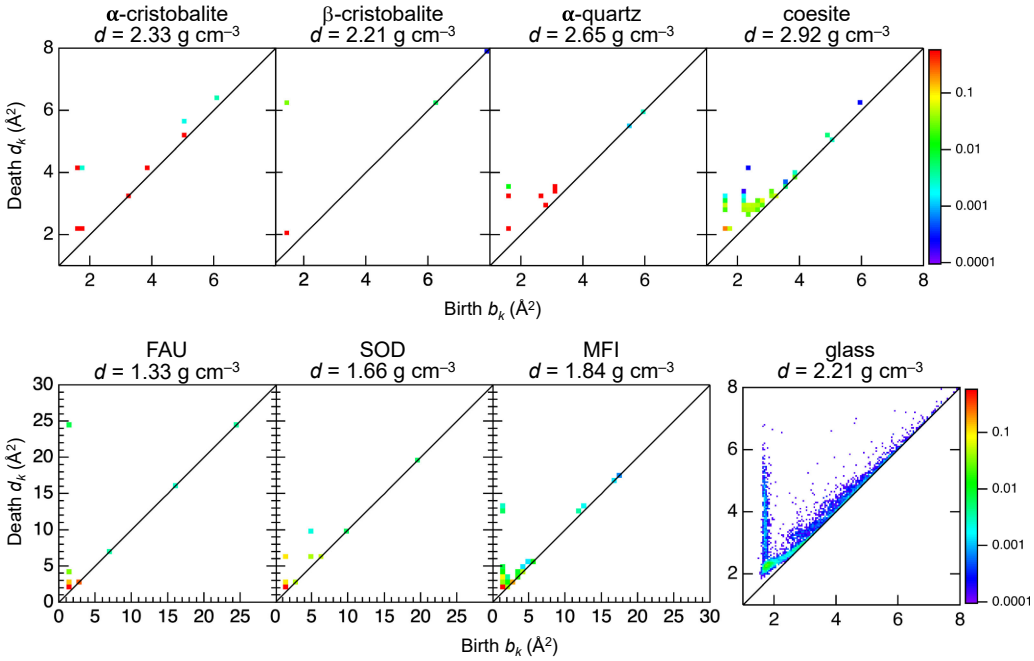

Fig. 8. O-centric PDs for a series of silica ploymorphs.[19] The prominent profile observed at $b_k/d_k \sim 1.6$ Å^2/2.2 Å^2 arises from threefold O–O–O rings in SiO_4 tetrahedra.

symmetrical cage is formed. MFI has an intermediate-size cage, as can be seen in the O-centric PD at $b_k/d_k \sim 1.4$ Å^2/13.0 Å^2, although the overall features of PDs for MFI are identical to that of SiO_2 silica glass. On the other hand, such a long lifetime profile can hardly be observed in the O-centric PD for SOD (Fig. 8). This feature for SOD can be seen in Fig. 4, in which no well-defined large cage structure is observed.

Figure S1 shows the tetrahedral order parameter q values of $SiSi_4$ tetrahedra for a series of silica polymorphs. β-cristobalite, which shows perfect hyper-tetrahedral coordination, has a q value larger than those of α-cristobalite, α-quartz, and coesite. On the other hand, siliceous zeolites exhibit an opposite behaviour. MFI has the largest q among these zeolites and significant broad distributions of q are observed in both the MFI and silica glass profiles,

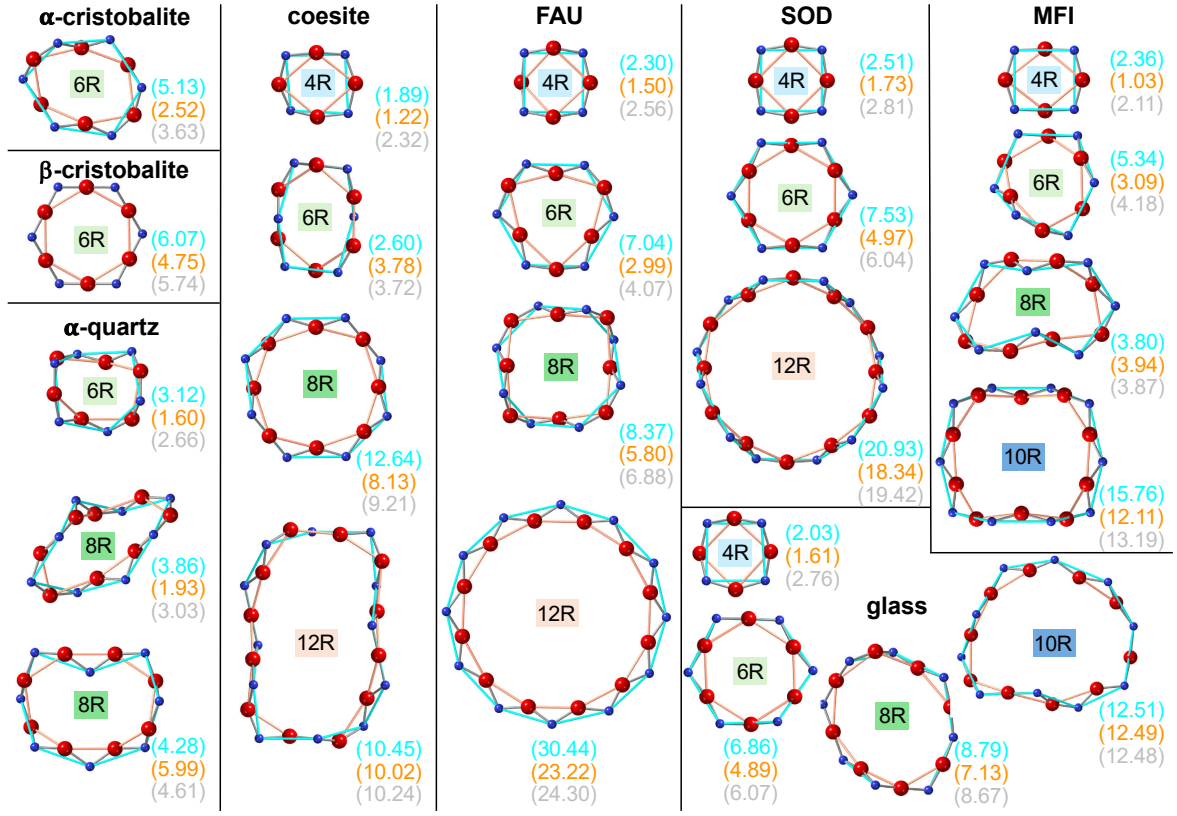

Fig. 9. Typical even-numbered $(Si–O)_n$ rings extracted from topological analyses of a series of silica polymorphs. Red sphere: oxygen; blue sphere: silicon. The conventional ring size distributions of a series of silica polymorphs are shown in Fig. S2.[19)]

which have comparable average q values of 0.89 and 0.84, respectively. This behaviour suggests that both MFI and silica glass are intermediate between crystalline silica and other siliceous zeolites. Small q values of FAU and SOD are presumably due to the large fraction of twelvefold ring (See Fig. S2).

Figure 9 shows typical even-numbered rings (cycles) obtained by a combination of ring size distribution and persistent homology analyses together with the lifetime of rings (cycles).[19)] This method enables us to measure the lifetime of each ring (cycle) on the basis of the Si–Si cycles, O–O cycles, and Si–O bonds. The rings (cycles) are represented by Si–Si bonds (orange), O–O bonds (cyan), and Si–O bonds (grey). The three values in parentheses are the lifetimes of each ring (cycle) calculated as $d_k - b_k$. The most universal feature is that oxygen atoms are buckled in $(Si–O)_n$ rings because the lifetime (shown in orange) is very short except in some symmetrical even-numbered rings, such as the sixfold rings in β-cristobalite, and large rings, such as the eightfold and twelvefold rings in coesite, tenfold rings in MFI, and twelvefold rings in SOD/FAU. Another remarkable feature is that the oxygen cycles of four-, six-, and eightfold ring have short lifetimes in MFI, which is the reason why MFI has the intetertrahedral O–O correlation despite its low density. On the other hand, the shapes of fourfold rings in coesite, FAU, SOD, and silica glass are identical. The $(Si–O)_6$ sixfold ring in β-cristobalite is very symmetrical owing to its long lifetime, which is different from the asymmetrical shape of the O–O cycle in α-cristobalite. We stress that this difference, manifested by the large d_k in the O-centric PD, is related to the formation of cavity with a small density difference between α-cristobalite ($d = 2.33\,\mathrm{g\,cm^{-3}}$) and β-cristobalite ($d = 2.21\,\mathrm{g\,cm^{-3}}$). Note that the sixfold rings in α-quartz are significantly buckled, those in MFI are slightly buckled, and those in coesite are rather symmetrical and squarish. On the other hand, the sixfold rings in FAU and SOD are very symmetrical, and those in glass are also very symmetrical similarly to β-cristobalite, although glass exhibits various ring shapes, as indicated by the broad profiles in the O-centric PDs. A similar trend is observed in the eightfold rings in α-quartz, FAU, MFI, and glass, but the eightfold rings in coesite are symmetrical despite having the highest density among the silica polymorphs as mentioned above. On the other hand, the twelvefold rings in FAU and SOD are very symmetrical and that in FAU exhibits the longest lifetime among the silica polymorphs. It is found that the shapes of the tenfold rings in MFI and glass are similar, although the fraction of such rings is not very large in the glass.

Figure 10 shows typical odd-numbered rings (cycles) in silica glass and MFI obtained by a combination of ring size distribution and persistent homology analyses together with the lifetime of each ring (cycle) based on the Si–Si cycles, O–O cycles, and Si–O bonds.[19)] It is found that the shapes of the fivefold and sevenfold rings in MFI are

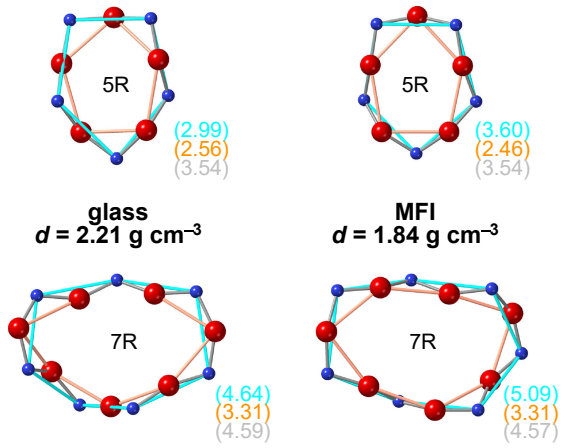

Fig. 10. Typical odd-numbered $(Si–O)_n$ rings extracted from topological analyses of silica glass and MFI.[19] Red sphere: oxygen; blue sphere: silicon. The rings (cycles) are represented by Si–Si bonds (orange), O–O bonds (cyan), and Si–O bonds (grey). The three values in parentheses are the lifetimes of each ring (cycle) calculated as $d_k - b_k$.

identical. Furthermore, similar shapes of rings can be ob served in silica glass. It is also found that oxygen atoms in both the fivefold and sevenfold rings are significantly buckled, which contributes to the local disorder in these structures.

A series of our topological analyses suggest that silica glass is crystallographically an analogue to β-cristobalite in terms of the diffraction peak position, as suggested by Gaskell and Wallis.[46] However, β-cristobalite is topologically ordered because it shows only sixfold rings,[19] in contrast to the topological disorder in silica glass. In this section, we compared silica crystals and glass with a series of siliceous zeolites in terms of topology and concluded that silica glass is topologically an analogue to MFI. As reported by Onodera and coworkers,[14,17] a series of topological analyses can clarify various hidden topologies, which cannot be detected in diffraction data. We consider that such hidden topologies are correlate with the functionality of oxide materials in terms of order within disorder.[48]

4. Conclusions

In this article, we chose several SiO_4 tetrahedral corner-sharing motif crystalline silica and siliceous zeolites in addition to the densified glasses of various densitiers. Using our approach, we found two descriptors for hyperordered structures in silica polymorphs.

The first descriptor of the hyperordered structure in silica glass can be expressed by the position and height of FSDP and PP. We investigated the behaviour of FSDP and PP by tuning pressure and temperature to obtain a systematic understanding of hyperorder. The second descriptor of hyperordered structures in silica polymorphs can be expressed in terms of topological characteristics: ring size distribution, cavity distribution, ring shape, and tetrahedral order without crystallographic information. We found an unusually large cavity volume in β-cristobalite and highly symmetrical eightfold and twelvefold rings in coesite. We also found a topological similarity between glass and MFI, in which fivefold and sevenfold rings are observed. A series of analyses demonstrate that the way to control topology is by tuning density through temperature and pressure treatments even where the synthesis processes for siliceous zeolites[49] are completely different from those for other silica polymorphs. Moreover, we demonstrate that the topological analyses provide us with the crucial key in understanding hyperordered structures in silica polymorphs.

Acknowledgements This work was partially supported by JSPS Grant-in-Aid for Transformative Research Areas (A) “Hyper-Ordered Structures Science” (Grant Numbers 20H05878 and 20H05881).

References

1) G. N. Greaves and S. Sen, *Adv. Phys.* 56, 1 (2007).
2) K. A. Kirchner, D. R. Cassar, E. D. Zanotto, M. Ono, S. H. Kim, K. Doss, M. L. Bødker, M. M. Smedskjaer, S. Kohara, L. Tang, M. Bauchy, C. J. Wilkinson, Y. Yang, R. S. Welch, M. Mancini and J. C. Mauro, *Chem. Rev.* 123, 1774 (2023).
3) S. Kohara and P. S. Salmon, *Adv. Phys.: X* 1, 640 (2016).
4) S. Kohara, *J. Ceram. Soc. Jpn.* 125, 799 (2017).
5) S. Kohara, *J. Ceram. Soc. Jpn.* 130, 531 (2022).
6) Y. Onodera, *J. Ceram. Soc. Jpn.* 130, 627 (2022).
7) K. Ohara, Y. Onodera, M. Murakami and S. Kohara, *J. Phys.-Condens. Mat.* 33, 383001 (2021).
8) S. Kohara and L. Pusztai, in “Computer Simulations of Glasses: Methodologies and Applications”, Ed. by J. Du and A. N. Cormack, Wiley-American Ceramic Society, Hoboken (2022) pp. 60–88.
9) S. Kohara, in “Hyperordered Structures in Materials: Disorder in Order and Order within Disorder”, Ed. by K. Hayashi, Springer Singapore, Singapore (2024) pp. 17–29.
10) D. L. Price, S. C. Moss, R. Reijers, M.-L. Saboungi and S. Susman, *J. Phys. C Solid State* 21, L1069 (1988).
11) A. C. Wright, *J. Non-Cryst. Solids* 179, 84 (1994).
12) P. S. Salmon, R. A. Martin, P. E. Mason and G. J. Cuello, *Nature* 435, 75 (2005).
13) P. S. Salmon and A. Zeidler, *J. Stat. Mech.-Theory E* 2019, 114006 (2019).
14) Y. Onodera, S. Kohara, S. Tahara, A. Masuno, H. Inoue, M. Shiga, A. Hirata, K. Tuchiya, Y. Hiraoka, I. Obayashi, K. Ohara, A. Mizuno and O. Sakata, *J. Ceram. Soc. Jpn.* 127, 853 (2019).
15) Q. Mei, C. J. Benmore, S. Sen, R. Sharma and J. Yargar, *Phys. Rev. B* 78, 144204 (2008).
16) S. Kohara, J. Akola, L. Patrikeev, M. Ropo, K. Ohara, M. Itou, A. Fujiwara, J. Yahiro, J. T. Okada, T. Ishikawa, A. Mizuno, A. Masuno, Y. Watanabe and T. Usuki, *Nat. Commun.* 5, 5892 (2014).
17) Y. Onodera, S. Kohara, P. S. Salmon, A. Hirata, N. Nishiyama, S. Kitani, A. Zeidler, M. Shiga, A. Masuno, H. Inoue, S. Tahara, A. Polidori, H. E. Fischer, T. Mori, S. Kojima, H. Kawaji, A. I. Kolesnikov, M. B. Stone, M. G. Tucker, M. T. McDonnell, A. C. Hannon, Y. Hiraoka, I. Obayashi, T. Nakamura, J. Akola, Y. Fujii,

K. Ohara, T. Taniguchi and O. Sakata, *NPG Asia Mater.* **12**, 85 (2020).
18) S. Sato, M. Miyakawa, T. Taniguchi, Y. Onodera, K. Ohara, K. Ikeda, N. Kitamura, Y. Idemoto and S. Kohara, *J. Ceram. Soc. Jpn.* **132**, 427 (2024).
19) S. Kohara, S. Sato, M. Shiga, Y. Onodera, H. Masai, T. Wakihara, A. Masuno, A. Hirata, N. Kitamura, Y. Idemoto, K. Kimura and K. Hayashi, *J. Ceram. Soc. Jpn.* **132**, 427 (2024).
20) I. Obayashi, T. Nakamura and Y. Hiraoka, *J. Phys. Soc. Jpn.* **91**, 091013 (2022).
21) Y. Hiraoka, T. Nakamura, A. Hirata, E. G. Escobar, K. Matsue and Y. Nishiura, *P. Natl. Acad. Sci. USA* **113**, 7035 (2016).
22) S. L. Roux and P. Jund, *Comp. Mater. Sci.* **49**, 70 (2010).
23) S. L. Roux and P. Jund, *Comp. Mater. Sci.* **50**, 1217 (2011).
24) I. Heimbach, F. Rhiem, F. Beule, D. Knodt, J. Heinen and R. O. Jones, *J. Comput. Chem.* **38**, 389 (2017).
25) I. Obayashi, *HomCloud*, https://homcloud.dev/index.en.html.
26) J. R. Errington and P. G. Debenedetti, *Nature* **409**, 318 (2001).
27) M. Shiga, A. Hirata, Y. Onodera and H. Masai, *Commun. Mater.* **4**, 91 (2023).
28) P. S. Salmon, A. Zeidler, M. Shiga, Y. Onodera and S. Kohara, *Phys. Rev. B* **107**, 144203 (2023).
29) M. Shiga, in "Hyperordered Structures in Materials: Disorder in Order and Order within Disorder", Ed. by K. Hayashi, Springer Singapore, Singapore (2024) pp. 265–288.
30) Y. Inamura, Y. Katayama, W. Utsumi and K. Funakoshi, *Phys. Rev. Lett.* **93**, 015501 (2004).
31) T. Sato and N. Funamori, *Phys. Rev. Lett.* **101**, 255502 (2008).
32) C. J. Benmore, E. Soignard, S. A. Amin, M. Guthrie, S. D. Shastri, P. L. Lee and J. L. Yarger, *Phys. Rev. B* **81**, 054105 (2010).
33) M. Murakami, S. Kohara, N. Kitamura, J. Akola, H. Inoue, A. Hirata, Y. Hiraoka, Y. Onodera, I. Obayashi, J. Kalikka, N. Hirao, T. Musso, A. S. Foster, Y. Idemoto, O. Sakata and Y. Ohishi, *Phys. Rev. B* **99**, 045153 (2019).
34) Y. Kono, K. Ohara, N. M. Kondo, H. Yamada, S. Hiroi, F. Noritake, K. Nitta, O. Sekizawa, Y. Higo, Y. Tange, H. Yumoto, T. Koyama, H. Yamazaki, Y. Senba, H. Ohashi, S. Goto, I. Inoue, Y. Hayashi, K. Tamasaku, T. Osaka, J. Yamada and M. Yabashi, *Nat. Commun.* **13**, 2292 (2022).
35) A. Zeidler, K. Wezka, R. F. Rowlands, D. A. J. Whittaker, P. S. Salmon, A. Polidori, J. W. E. Drewitt, S. Klotz, H. E. Fischer, M. C. Wilding, C. L. Bull, M. G. Tucker and M. Wilson, *Phys. Rev. Lett.* **113**, 135501 (2014).
36) M. Guerette, M. R. Ackerson, J. Thomas, F. Yuan, E. B. Watson, D. Walker and L. Huang, *Sci. Rep.-UK* **5**, 15343 (2015).
37) M. Grimsditch, *Phys. Rev. Lett.* **52**, 2379 (1984).
38) C. Meade and R. Jeanloz, *Phys. Rev. B* **35**, 236 (1987).
39) J. Haines, C. Levelut, A. Isambert, P. Hébert, S. Kohara, D. A. Keen, T. Hammouda and D. Andrault, *J. Am. Chem. Soc.* **131**, 12333 (2009).
40) H. Masai, S. Kohara, T. Wakihara, Y. Shibazaki, Y. Onodera, A. Masuno, S. Sukenaga, K. Ohara, Y. Sakai, J. Haines, C. Levelut, P. Hébert, A. Isambert, D. A. Keen and M. Azuma, *Commun. Chem.* **6**, 269 (2023).
41) K. Goetzke and H. J. Klein, *J. Non-Cryst. Solids* **127**, 215 (1991).
42) X. Yuan and A. N. Cormack, *Comp. Mater. Sci.* **24**, 343 (2002).
43) A. R. Cooper, *Phys. Chem. Glasses* **19**, 60 (1978).
44) R. L. McGreevy and L. Pusztai, *Mol. Simulat.* **1**, 359 (1988).
45) C. J. Benmore and M. C. Wilding, *Elements* **17**, 175 (2021).
46) P. H. Gaskell and D. J. Wallis, *Phys. Rev. Lett.* **76**, 66 (1996).
47) A. Zeidler, P. S. Salmon and L. B. Skinner, *P. Natl. Acad. Sci. USA* **111**, 10045 (2014).
48) P. S. Salmon, *Nat. Mater.* **1**, 87 (2002).
49) B. Li, K. Iyoki, P. Techasarintr, S. Elangovan, R. Simancas, T. Okubo, T. Yokoi and T. Wakihara, *ACS Catal.* **13**, 15155 (2023).